

GEOCHEMICAL FEATURES, ISOTOPE COMPOSITIONS AND ENVIRONMENTAL IMPACTS OF HOT SPRINGS IN KEJIE FAULT AND CHANGNING-MENGLIAN STRUCTURAL BELT

BA, J. J. – LYU, Y. * – PAN, M. – ZHANG, Q. Y. – LIANG, B.

*Institute of Karst Geology, CAGS/Key Laboratory of Karst Dynamics, MNR&GZAR
Guilin 541004, China*

**Corresponding author
e-mail: lvy@karst.ac.cn*

(Received 18th Mar 2019; accepted 17th May 2019)

Abstract. To disclose the exact geochemical features of the hot springs in western Yunnan, China, this paper reviews the geological settings of Changning County, western Yunnan, and analyzes the geochemical features of local hot springs, which are controlled by Kejie Fault and Changning-Menglian (C-M) Structural Belt. On this basis, the author explored the isotopes of H, O, C, recharge source, recharge elevation circulation path and formation age of the geothermal flow, examined the main chemical process in the geothermal flow movement, especially in the mixing process, and determined the geochemical formation model and geological settings of the fault-controlled geothermal field in the research area. The results show that the hot springs are typical fault-controlled geothermal resources; the meteoric water is the main supply source of the hot springs; the hot springs are neither volcanic nor magmatic; despite the slight difference in activities and formation causes, the hot springs in both western and eastern parts of the research area were recharged by paleo-precipitation recharge before Late Pleistocene.

Keywords: *hot springs, isotopes, formation model, geothermal resources, western Yunnan, China*

Introduction

The world boasts huge reserves of geothermal energy, which promises efficient, stable power generation. If properly utilized, geothermal energy could promote energy conservation, reduce carbon emissions and mitigate global warming (Ahmadi et al., 2018; Ba et al., 2018; Mawarni et al., 2018). China is the second largest holder of geothermal reserves, most of which exist in tectonically active belts and large sedimentary basins (Wang et al., 2000; Guo, 2012). In general, there are abundant low-temperature geothermal resources in the uplift and subsidence areas of the continental crust, and some high-temperature ones across Yunnan and Tibet in southwestern China (Guo et al., 2013).

In the border areas between Tibet and Yunnan, the heat state of lithosphere has been shaped by the tectonically extrusion of the southeastern edge of Qinghai-Tibet Plateau since the Cenozoic era. The heat flow in this region far exceeds 70 mW/m², and peaks at 120.5 mW/m² in Tengchong, western Yunan Province, twice the global mean value (61.6 mW/m²) (Du et al., 2005), revealing the typical geothermal features of a modern tectonically active area. The regional distribution of heat flow, especially that of abnormally high geo-temperature, is highly consistent with the pattern of deep faults.

The deep faults control the regional structure framework, affecting the formation and distribution of secondary structural belts. For example, the fault-controlled geothermal resources in western Yunnan possess the following features: large scale, shallow burial and high temperature (Mongillo, 2010; Ba et al., 2018). These faults also create a good

condition for magma intrusion and convection (Edmunds, 2004; Olivier et al., 2011) and a passageway to the heat sources deep in the mantle, providing favorable paths for hot springs (Brown et al., 2003; Lachenbruch et al., 2013; Awaleh et al., 2015). In the said region, there are 139 hot springs with temperatures above 150°C, including 49 (35.3%) in western Yunnan. Many of them correspond with the hydrothermally active spots along the Kejie Fault and its secondary faults.

Over the years, some scholars have explored the distribution features, heat control mechanism and conformation model of Keijie Fault and the nearby Changning-Menglian (C-M) Structural Belt in western Yunnan (Wang et al., 2000; Guo, 2012; Ba et al., 2018). However, none of them has explained the exact geochemical features of the hot springs in this region, not to mention creating a conformation model of the local geothermal field.

To fill in these gaps, this paper reviews the geological settings of Changning County, western Yunnan, analyzes the chemical features of local hot springs, namely, hydro-chemical type, phase equilibrium, water-rock interaction, flow runoff and isotope features, and discusses about the isotopes of H, O, C, recharge source, supply elevation circulation path and formation age of the geothermal flow. In addition, the author examined the main chemical process in the geothermal flow movement, especially in the mixing process, and finally determined the geochemical formation model and geological settings of the fault-controlled geothermal field in the research area.

Materials and methods

Geological background

Located in Changning County, western Yunnan, the research area is high in the north and low in the south, with mountains and river valleys spanning in the north-south direction. In the west of the research area lies a U-shaped basin (elevation: 840~2,525 m) along the Kejie Fault, where the annual mean temperature is 19.5°C and the annual precipitation is 960 mm. In the eastern part, there is the Changning Basin (elevation: 1,562~2,525 m), where the climate is moderate and humid, the annual mean temperature is 14.9°C and the annual precipitation is 1,253.1 mm.

From the perspective of tectonics, the research area belongs to Baoshan Block, a part of the Yunnan-Burma-Thailand-Malaysia microplate, and falls between the C-M Structural Belt and the Yangtze Block (*Figure 1a*). The C-M Structural Belt is formed through the collision between two microcontinents within the remnant Paleo-Tethys Ocean realm. Despite the complex tectonics, the internal structure of the structural belt can be clearly identified (Xu et al., 2016).

Geological settings of Kejie Fault

Kejie Fault is an important fault in western Yunnan, controlling the sedimentation, metamorphism and magmatic activities since the Early Paleozoic era. The control effect is particularly prominent in Late Paleozoic Era. During the Lancang Orogeny, the fault appeared in the junction between Baoshan Block and C-M Structural Belt, and controlled the stratigraphic sedimentation for a longtime before the Permian era.

Kejie Fault consists of a primary fault and two secondary faults. The north-south primary fault spans 1,000 m in 20° east of north from Kejie Town to Kasi Town, and dips steeply towards the east by 60°~90°. The two secondary faults extend from north to

northwest, and intersect the primary fault at acute angles. Numerous hot springs (S1~S7) are exposed along the two secondary faults (*Figure 1b*).

There is a 200~500 m wide breccia fracture zone within the Kejie Fault, as well as a north-south fold deformation zone in the northwest part. The metamorphic rocks are $90^\circ \angle 40^\circ$ on the eastside, which intersects the fault at an acute angle. The Yanshanian acidic intrusive rocks are also deformed, becoming schistous and partly mylonitic. Many places of the fault are hidden under the Quaternary sediments, forming continuous gullies and beaded Cenozoic sedimentary basins with obvious neo-tectonic features.

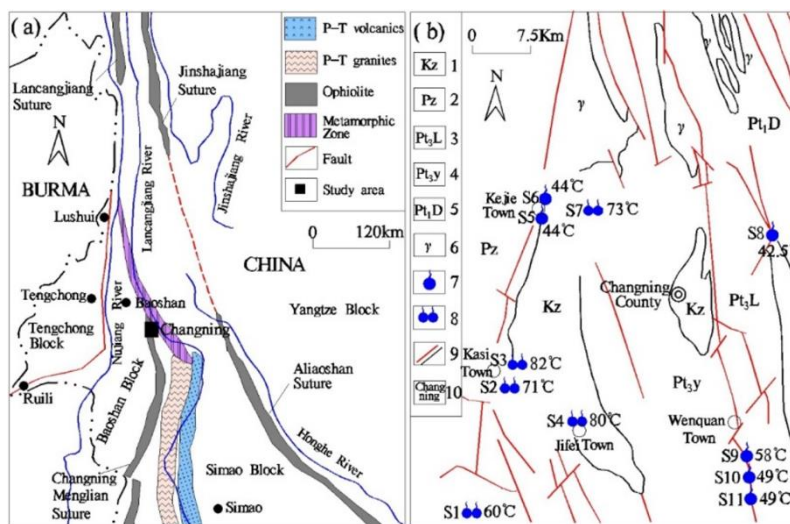


Figure 1. (a) Geological sketch map of western Yunnan; (b) Hot springs

Note: 1-Cenozoic Erathem; 2-Paleozoic Erathem; 3- Proterozoic Lancang Formation; 4-Proterozoic Yungou Formation; 5- Proterozoic Damenglong Formation ; 6-Granite; 7-Hot spring; 8-Group of hot springs; 9-Boundary of Fault and stratigraphic boundaries; 10-Changning County; S1: Kasihe Hot Spring Group; S2: Liangyuan Hot Spring Group; S3: Ganlanhe Hot Spring Group; S4: Jifei Hot Spring Group; S5: Dadi Hot Spring; S6: Suanxi Hot Spring; S7: Yudili Hot Spring Group; S8: Xiazhai Hot Spring; S9 Qingyunge Hot Spring; S10: Xiaoqiao Hot Spring; S11: chenjia Hot Spring

Geological settings of C-M Structural Belt

The 10~60 km-wide C-M Structural Belt runs through the research area from the northwest to the south. The belt has been shaped like a narrow wedge in the northwest, adjacent to Xiqianjie Fault and Baoshan- Zhenkang Block in the west, and bordered by Lancangjiang Fault and Yangtze Block in the east. Many hot springs are exposed along the belt in Wenquan Town, southern Changning County.

As a remnant of the C-M ocean basin, the belt mainly consists of Carboniferous metabasites, volcanic rocks, altered diabases and a few low-grade metamorphic siltstones. The rock stratum includes Proterozoic Damenglong Formation, Neoproterozoic Lancang Formation, Devonian Wenquan Formation, Devonian Pingzhang Formation, Devonian- Carboniferous Nanduan Formation and Permian Laba Formation. There are also a few acidic volcanic rocks of Triassic Huaimang Formation, molasses deposit of Triassic Sanchahe Formation, and clastic deposits in continental basins of Pliocene Mangbang Formation.

Sample analysis

A total of 19 geothermal water samples were acquired from the research area, including 4 samples collected by delta δD , 4 by delta $\delta^{18}O$, 4 by δ^3H , 2 by $\delta^{14}C$ and 5 by $\delta^{13}C$. All water samples were stored in low-density polyethylene bottles without any special pretreatment. Among them, δ^3H , $\delta^{18}O$ and $\delta^{14}C$ samples were measured on a MAT253 isotope ratio mass spectrometer, and $\delta^{13}C$ samples on a stable isotope ratio mass spectrometer (SIRMS), with the aid of acid hydrolysis.

For hydro-chemical analysis of ions, the 50 mL polyethylene sampling bottles were filled up with $\delta^3H_{H_2O}$ and $\delta^{18}O_{H_2O}$ samples, to prevent the formation of bubbles. The cations (Ca^{2+} , Mg^{2+} , Na^+ , and K^+) were analyzed on an AA-100 atomic absorption spectrometer, after super pure HNO_3 (1:1) had been added to the samples until the pH value fell below 2. The HCO_3^- was titrated by an alkalimeter with precision of 0.1 mmol/L, the pH of the water was determined by a WTW Multi3430 multiparameter meter with precision of 0.01. The anions (SO_4^{2-} , Cl^- , and NO_3^-) were measured through high-performance liquid chromatography.

All water samples were analyzed at the Institute of Karst Geology, Chinese Academy of Geological Sciences.

Results

The geothermal resources in the research area mainly exist in the fault zone amidst fold mountains. Most of them are of medium to low temperature. As shown in *Figure 1b*, the research area can be divided into Kejie Town area in the west (the western part) and Wenquan Town area in the east (the eastern part).

Geothermal control area in Kejie Fault

Geochemical features and formation conditions of the hot springs in Kejie Town area

As mentioned in Section 2, the geothermal sources in Kejie Fault are controlled by the primary and secondary faults. At the intersections between the faults, the clastic sediments in the Cenozoic depression provide a good thermal cover for the geothermal reservoirs. Several hot springs are exposed in the western part of the research area. Seven of them were selected for investigation. As shown in *Table 1*, the temperature of every spring is above 40°C (the temperature of the hottest spring: 90°C) and the total flow rate of these springs reaches 11.56 L/s (the flow rate of the fastest flowing spring: 3.42 L/s).

Table 1. Flow rates and temperatures of the hot springs in the western part

Area	Tepid hot springs				High temperature hot springs		Medium-high temperature hot springs		Low temperature hot springs	
	Spots	Flow rate (L/s)	High temperature (°C)	Low temperature (°C)	Spots	Flow rate (L/s)	Spots	Flow rate (L/s)	Spots	Flow rate (L/s)
Kejie Town	7	11.56	90	44	1	1.47	6	10.09	-	-
Wenquan Town	3	13.90	58	23	-	-	2	6.54	1	7.36

Most of the water samples appear at the bottom of the Piper trilinear diagram of hydro-chemical ions (*Figure 2*). Obviously, the main cations in the water samples are Na^+ , Ca^{2+} and K^+ , and their contents differ from spring to spring. The water in S5 belongs to the Ca-Na type, with a high content of Ca^{2+} ; the water in S3 belongs to the Na-K type, with greater-than-90% contents of Na^+ and K^+ ; the water in the other springs belongs to the Na-Ca type. The high content of Ca^{2+} in these hot springs can be attributed to the geothermal interaction between water and rock.

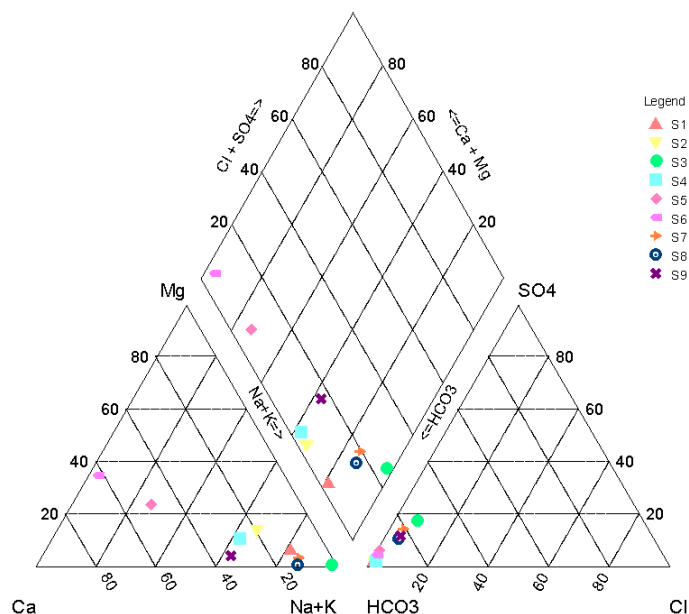


Figure 2. The Piper trilinear diagram of hydro-chemical ions of the hot springs in the western part

Since all samples appear at the bottom left of the Piper diagram on anions, HCO_3^- is the dominant anion in all the water samples. In particular, the HCO_3^- contents in S2 and S5 are over 90%, while those of Cl^- and SO_4^{2-} are below 10%. Of course, the springs differ in the exact content of HCO_3^- , due to the varied degrees of carbonate decomposition.

Below is a brief analysis of the ion contents in four of the seven hot springs: S2, S3, S4 and S7.

S2: This group of hot springs is located on the Kejie Fault, with a complete generation-reservoir-cover system. The reservoir stratum is the footwall in the west of the fault, which consists of broken quartz sandstone, siltstone of Xiangyangsi Formation, Lower Devonian Series (D_{1x}), while the cover stratum is the hanging wall of semi-consolidated conglomerate and argillaceous siltstone of Mangbang Formation Pliocene Series (N_{2m}). As shown in *Table 2*, HCO_3^- (973.75 mg/L) is the dominant anion in S2, accounting for 97.7% of anions in the spring water; other anions like Cl^- and SO_4^{2-} have a very low presence. Na^+ and K^+ are the main cations, taking up 74.84% of all cations in the spring water, while the Ca^{2+} content stands at 17.53%. Meanwhile, the total dissolved solid (TDS) is as high as 938.12 mg/L.

S3: On the north of Ganlahe valley, this group of 10 hot springs belongs to the Yungou Formation, Neoproterozoic Nanhua Series. This formation mainly consists of

regional low-grade metamorphic rocks like sericite-phyllite. Under the intrusion of Cretaceous biotite adamellite, the rocks have partially evolved into thermal metamorphic hornfels. The formation is well developed, with a secondary joint parallel to the north-northwest fault. The total flow rate of S3 stands at 8.0 L/s (the flow rate of the fastest-flowing spring is 2.5 L/s), and the temperature at the spring mouths reaches 82°C (Table 2). The spring water is colorless and transparent, and belongs to the hydro-chemical type of HCO₃-Na+K, owing to the few travertines at the spring mouths.

Table 2(a). Common hydro-chemical features of the hot springs in the western part

Sample (No.)	T (°C)	Common Cation (mg/L)				
		K ⁺	Na ⁺	Ca ²⁺	Mg ²⁺	NH ₄ ⁺
Kasihe (S1)	60.0	28.1	254.0	35.8	11.7	1.10
Liangyuan (S2)	71.0	65.0	219.8	66.7	28.0	1.05
Ganlanhe (S3)	82.0	1.5	89.1	1.5	0.2	0.03
Jifei (S4)	90.0	20.3	162.4	65.6	14.9	2.65
Dadi (S5)	44.0	6.0	69.7	121.8	34.6	<0.02
Suanxi (S6)	44.0	1.4	4.1	75.4	25.4	<0.02
Yudili (S7)	73.0	9.1	111.6	13.4	2.2	3.23
Xiazhai (S8)	42.5	1.0	47.8	6.4	0.1	0.29
Qingyunge (S9)	58.0	11.0	129.2	63.0	4.4	1.94

Table 2(b). Common hydro-chemical features of the hot springs in the western part

Sample (No.)	T (°C)	Common anions (mg/L)						
		Cl ⁻	SO ₄ ²⁻	HCO ₃ ⁻	CO ₃ ²⁻	F ⁻	NO ₃ ⁻	NO ₂ ⁻
Kasihe (S1)	60.0	6.04	11.86	843.18	0	1.88	1.31	0.006
Liangyuan (S2)	71.0	9.13	11.17	973.75	0	0.86	1.27	0.034
Ganlanhe (S3)	82.0	5.55	16.15	91.24	25	20.73	1.09	0.010
Jifei (S4)	90.0	8.28	8.55	706.32	0	3.58	1.06	<0.002
Dadi (S5)	44.0	2.80	31.57	654.41	0	1.46	1.09	<0.002
Suanxi (S6)	44.0	1.49	11.97	335.07	0	0.73	2.22	<0.002
Yudili (S7)	73.0	9.75	37.23	270.57	0	12.80	1.06	<0.002
Xiazhai (S8)	42.5	2.30	5.89	62.92	31	3.94	1.07	<0.002
Qingyunge (S9)	58.0	16.62	50.11	471.93	0	5.55	1.06	<0.002

S4: This group of 18 springs is exposed in the valley and restricted by the northwestern fault, featuring a complete generation-reservoir-cover system. The reservoir stratum is mainly made up of volcanic rocks (dacite liparite) in the Triassic Manghuai Formation, while the cover stratum is semi-consolidated conglomerate and argillaceous siltstone of Pliocene Mangbang Formation (N₂m). The temperature of spring water falls between 42 and 80°C, and that of the hottest spring mouth reaches 90°C (higher than the local boiling point of water (Table 2).

S7: The geothermal resource in this group of springs is deep circulating and low in temperature, due to the well-developed, complex fault nearby. The stratum belongs to Yungou Formation, Neoproterozoic Nanhua Series, which encompasses regional low-

grade metamorphic rocks like sericite-phyllite and mic schist. The spring group is exposed in the east-west secondary fracture, which is perpendicular to the main fault. The flow rate and temperature of S7 are respectively 3.42L/s and 73°C (Table 2). The spring water belongs to the hydro-chemical type of HCO₃-Na (Table 2), due to the thick travertines around the spring mouths. The TDS is 0.47 g/L, consisting of F, SiO₂, As, Mn, HPO₄, etc. Both H₂S and SiO₂ exist in the spring water, in which the SiO₂ content (124.52 mg/L) far exceeds the standard for mineral water.

According to the hydro-chemical features, the Schoeller plots of the hot springs in the western part were drawn on AquaChem (Figures 3 and 4). These plots show that the different ions have similar trend in content in the water samples of different hot springs. This means these springs are recharged by the same reservoir source and formed under the same conditions, forming similar fault-controlled geothermal resources.

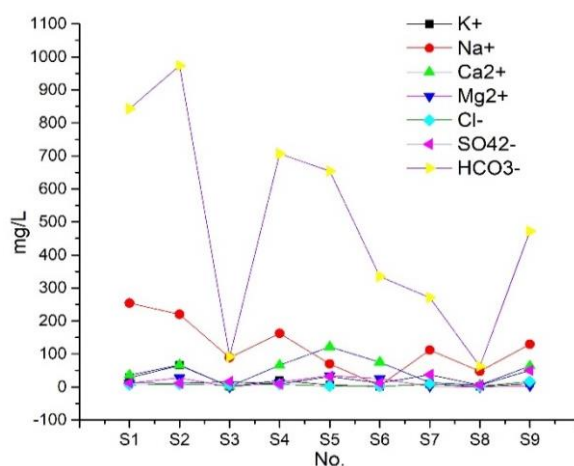


Figure 3. Main ion contents of the hot springs in the western part

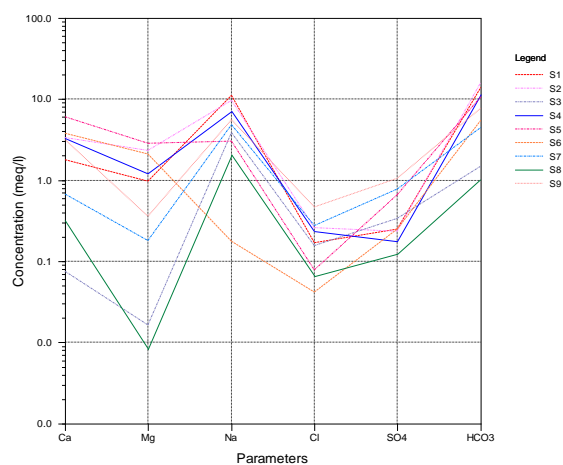


Figure 4. Schoeller plots of the hot springs in the western part

In addition, F⁻ anions were observed in the water of the hot springs in the western part. These anions are produced through the weathering of tourmaline, mica and apatite

in geothermal reservoirs. The content of F^- in the spring water has many to do with the groundwater type, lithological features of surrounding rocks, degree of water-rock interaction and environmental temperature. The pH and flow temperature are the leading influencing factors of the content. As shown in *Figure 5*, the F^- content is positively correlated with the temperature of the exposed hot springs.

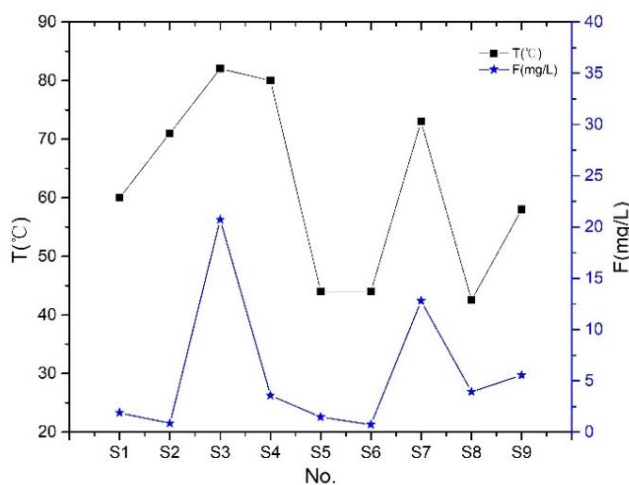


Figure 5. Relationship between temperature and F^- content of the hot springs in the western part

Potential environmental impacts of the hot springs in the western part

The heavy metal contents of these hot springs were measured. The results show that the spring water enjoys an overall good quality, and can be exploited as geothermal resources. The contents of trace elements in the spring water are listed in *Table 3* below.

Table 3(a). Trace elements of the hot springs in the western part

Sample (No.)	Trace elements (mg/L)					
	Zn	Co	Mn	As	Hg	TFe
Kasihe (S1)	<0.002	<0.002	0.056	<0.002	<0.0001	0.014
Liangyuan (S2)	<0.002	<0.002	0.082	0.007	<0.0001	0.220
Ganlanhe (S3)	<0.002	<0.002	0.0022	<0.002	<0.0001	0.015
Jifei (S4)	<0.002	<0.002	0.046	<0.002	<0.0001	0.007
Dadi (S5)	<0.002	<0.002	0.011	0.014	<0.0001	0.110
Suanxi (S6)	<0.002	<0.002	<0.001	<0.002	<0.0001	0.005
Yudili (S7)	<0.002	<0.002	0.049	<0.002	<0.0001	0.016
Xiazhai (S8)	<0.002	<0.002	<0.001	<0.002	<0.0001	0.004
Qingyunge (S9)	<0.002	<0.002	0.026	0.004	<0.0001	0.120

It can be seen that the spring water has high contents of As, Mn, and Hg (2.0~14.0 $\mu\text{g/L}$, 11.0~82.0 $\mu\text{g/L}$ and 0.1 $\mu\text{g/L}$, respectively). The As content in S5 (14.00 $\mu\text{g/L}$) hot springs is much higher than that (2.0~7.0 $\mu\text{g/L}$) in any other spring. This may be the result of the leaching after water-rock interaction.

Table 3(b). Trace elements of the hot springs in the western part

Sample (No.)	Special Projects (mg/L)					
	SiO ₂	Free CO ₂	PO ₄ ³⁻	Hydrochemical types	Water hardness	pH
Kasihe (S1)	92.09	5.62	<0.02	HCO ₃ -Na·Ca	137.72	7.61
Liangyuan (S2)	48.26	7.49	0.07	HCO ₃ -Na·Ca	281.80	6.99
Ganlanhe (S3)	73.58	0.00	<0.02	HCO ₃ -Na	4.40	8.95
Jifei (S4)	70.37	9.37	<0.02	HCO ₃ -Na·Ca	224.95	6.67
Dadi (S5)	30.33	9.37	0.03	HCO ₃ -Ca·Na	446.70	6.64
Suanxi (S6)	16.02	5.62	<0.02	HCO ₃ -Ca	292.96	7.43
Yudili (S7)	117.22	3.75	<0.02	HCO ₃ -Na	42.49	7.70
Xiazhai (S8)	42.65	0.00	<0.02	HCO ₃ -Na	16.11	9.17
Qingyunge (S9)	89.97	5.62	<0.02	HCO ₃ -Cl-Na·Ca	175.41	7.31

Geochemical-chronological features of carbon, hydrogen and oxygen isotopes of the hot springs in the western part

The hot springs S2~S5 and S7 were subjected to isotopic analysis on $\delta D_{(V-SMOW)}$, $\delta^{18}O_{(V-SMOW)}$, $^3H_{(TU)}$, dissolved inorganic carbon $\delta^{13}C_{DIC(V-PDB)}\%$, particulate organic carbon $\delta^{13}C_{POC(V-PDB)}\%$ and dissolved organic carbon $\delta^{13}C_{DOC(V-PDB)}\%$. The results in Tables 4 and 5 show that δD , $\delta^{18}O$ and 3H fall in the ranges of $-79.1\sim-84.2$, $-10.66\sim-11.76$ and <2 , respectively; the $\delta^{13}C_{DIC}$, $\delta^{13}C_{POC}$ and $\delta^{13}C_{DOC}$ fall in the ranges of $-1.37\sim-4.24$, $-15.88\sim-27.08$ and $-24.62\sim-31.16$, respectively; The $\delta D_{(V-SMOW)}$, $\delta^{18}O_{(V-SMOW)}$, $\delta^{13}C_{DIC(V-PDB)}\%$ and $\delta^{13}C_{POC(V-PDB)}\%$ average at -81.62 , -2.32 , -2.04 and -22.84 , respectively. In addition, only S2 has a positive value of $\delta^{13}C_{DIC}$, as shown in Figure 6.

Table 4. Isotopic test results on $\delta D_{(V-SMOW)}$, $\delta^{18}O_{(V-SMOW)}$ and $^3H_{(TU)}$ of the hot springs in the western part

Name (No.)	$\delta D_{(V-SMOW)}\%$	$\delta^{18}O_{(V-SMOW)}\%$	$^3H_{(TU)}$
Liangyuan (S2)	-82.1	-11.34	<2
Ganlanhe (S3)	-82.5	-11.58	<2
Jifei (S4)	-84.2	-11.26	<2
Dadi (S5)	-79.1	-10.66	<2

Table 5. Isotopic test results on $\delta^{13}C_{DIC(V-PDB)}\%$, $\delta^{13}C_{POC(V-PDB)}\%$ and $\delta^{13}C_{DOC(V-PDB)}\%$ of the hot springs in the western part

Name (No.)	Sample Type	$\delta^{13}C_{DIC(V-PDB)}\%$	$\delta^{13}C_{POC(V-PDB)}\%$	$\delta^{13}C_{DOC(V-PDB)}\%$
Liangyuan (S2)	water sample	1.37	-27.08	-24.62
Ganlanhe (S3)	water sample	-4.24	-15.88	-31.16
Jifei (S4)	water sample	-1.82	-26.69	-
Dadi (S5)	water sample	-3.45	-25.28	-
Yudili (S7)	water sample	-2.04	-19.27	-29.58

It can also be seen that the pH values of these hot springs range between 6.64 and 8.95 (Table 3); the dissolved inorganic carbon exists as HCO₃⁻, such that the $\delta^{13}C_{DIC}$ value is basically the same as $\delta^{13}C_{HCO_3^-}$.

Furthermore, the S4 hot spring received ^{14}C isotopic dating (half-life period: 5,730 a), which puts its age at $16,510 \pm 1,600\text{a}$. The result indicates that S4 received paleo-precipitation recharge before Late Pleistocene. The temperature of S4 can reach 90°C , an evidence of good geothermal property and a closed supply condition.

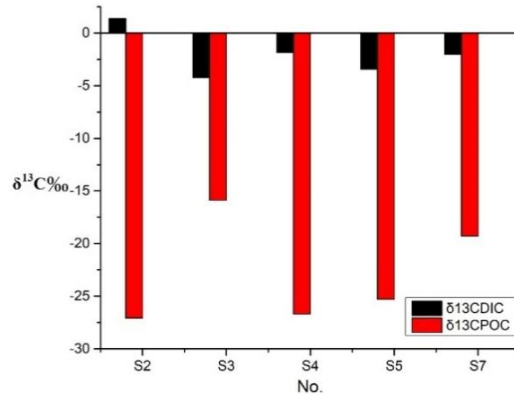


Figure 6. $\delta^{13}\text{C}_{\text{DIC}}$ of the hot springs in the western part

Geothermal control area in C-M Structural Belt

Geochemical features of hot springs in the eastern part

In the eastern part of the research area, the distribution of hot springs is mainly controlled by the C-M structural belt. The typical hot springs in this area are S8~S10. Here, S10 is selected as an example to analyze the geochemical features of hot springs in the eastern part of the research area.

The S10 spring group is exposed on the west side of the valley. The stratum mainly consists of sericite and marble in Pingzhang Formation, Carboniferous system (C_{1pz}). In terms of nappe structure, the stratum thrusts itself up the intermontane conglomerate and interbedded sandstone and mudstone of Triassic Sanchahe Formation (T_{3sc}). Thus, the underground geothermal water encounters the T_{3sc} layer and becomes exposed on the ground (Figure 7).

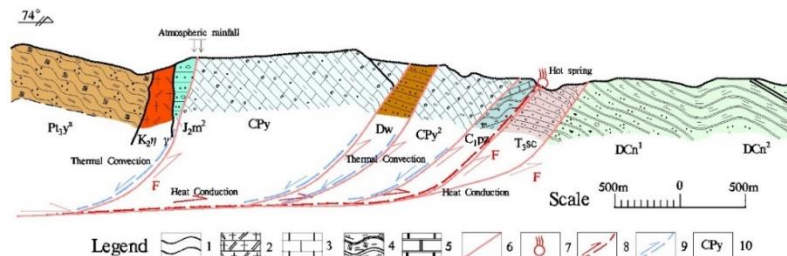


Figure 7. Hydrothermal circulation of S10

Note: 1-Schist; 2-Adamellite; 3-Limestone; 4-Slate; 5-Marble; 6-Fault; 7-Hot springs; 8-Geothermal water migration path; 9-Recharge water migration path; 10-Stratigraphic age

For the four-mouth spring group, the total flow rate stands at 11.9 L/s (the flow rate of the fastest flowing mouth is 2.3 L/s), and the temperature falls between 23 and 65°C . With pale yellow sulfur deposits and obvious H_2S gas around some mouths, the spring

group belongs to the hydro-chemical type of $\text{HCO}_3\text{-Na}\cdot\text{Ca}$, the TDS is 0.57 g/L. The contents of F^- and SiO_2 are 5 mg/L and 88.7 mg/L, respectively. In summary, the spring water of S10 fits in with the definition of mineral water.

Geochemical-chronological features of carbon, hydrogen and oxygen isotopes of the hot springs in the eastern part

The hot springs S8~S10 were subjected to isotopic analysis on $\delta\text{D}_{(\text{V-SMOW})}$, $\delta^{18}\text{O}_{(\text{V-SMOW})}$, $^3\text{H}_{(\text{TU})}$, $\delta^{13}\text{C}_{\text{DIC}(\text{V-PDB})}\text{‰}$, $\delta^{13}\text{C}_{\text{POC}(\text{V-PDB})}\text{‰}$ and $\delta^{13}\text{C}_{\text{DOC}(\text{V-PDB})}\text{‰}$. The results in *Tables 6 and 7* show that $\delta\text{D}_{(\text{V-SMOW})}$, $\delta^{18}\text{O}_{(\text{V-SMOW})}$ and $^3\text{H}_{(\text{TU})}$ fall in the ranges of $-78.1\sim-85.8$, $-10.76\sim-11.81$ and < 2 , respectively. The $\delta^{13}\text{C}_{\text{DIC}(\text{V-PDB})}\text{‰}$, $\delta^{13}\text{C}_{\text{POC}(\text{V-PDB})}\text{‰}$ and $\delta^{13}\text{C}_{\text{DOC}(\text{V-PDB})}\text{‰}$ amount to $-0.90\sim-9.26$, -23.54 and $-25.66\sim-28.90$, respectively. These results are similar with those of the hot springs in the western part, except for the smaller fraction of biogenic water. This means geothermal water in the eastern part circulates deeper than that in the western part.

Table 6. Isotopic test results on $\delta\text{D}_{(\text{V-SMOW})}$, $\delta^{18}\text{O}_{(\text{V-SMOW})}$ and $^3\text{H}_{(\text{TU})}$ of the hot springs in the eastern part

Name (No.)	$\delta\text{D}_{(\text{V-SMOW})}\text{‰}$	$\delta^{18}\text{O}_{(\text{V-SMOW})}\text{‰}$	$^3\text{H}_{(\text{TU})}$
Xiazhai (S8)	-85.8	-11.81	<2
Qingyunge (S9)	-78.1	-10.76	<2

Table 7. Isotopic test results on $\delta^{13}\text{C}_{\text{DIC}(\text{V-PDB})}\text{‰}$, $\delta^{13}\text{C}_{\text{POC}(\text{V-PDB})}\text{‰}$ and $\delta^{13}\text{C}_{\text{DOC}(\text{V-PDB})}\text{‰}$ of the hot springs in the eastern part

Name (No.)	$\delta^{13}\text{C}_{\text{DIC}(\text{V-PDB})}\text{‰}$	$\delta^{13}\text{C}_{\text{POC}(\text{V-PDB})}\text{‰}$	$\delta^{13}\text{C}_{\text{DOC}(\text{V-PDB})}\text{‰}$
Xiazhai (S8)	-9.26	-23.54	-28.90
Qingyunge (S9)	-0.90	-	-25.66

In addition, the hot springs in the eastern part received ^{14}C isotopic dating (half-life period: 5,730 a), which puts their ages at $17,220\pm 550\text{a}$. The result indicates that the hot springs received paleo-precipitation supply before Late Pleistocene. The geothermal water circulated slowly and formed the springs before S4.

Discussion

Mixing features of hot water and cold water

The geothermal water is inevitably mixed with cold water as it rises to the surface. The fractions of cold water in S3, S4, S7 and S10 were computed, and recorded in *Figure 8*, where the ordinate value of the intersection between curves X_t and X_{si} stands for the theoretical fraction of cold water.

As shown in the figure, the cold-water fractions of S3, S4, S7 and S10 are 66%, 67%, 77% and 70%, respectively. Meanwhile, the temperatures of S3, S4, S7 and S10 are 175°C, 176°C, 250°C and 200°C, respectively. Hence, the cold-water fraction is positively correlated to temperature. Similarly, the cold-water fraction and temperature of S2 were computed as 53% and 130°C, respectively.

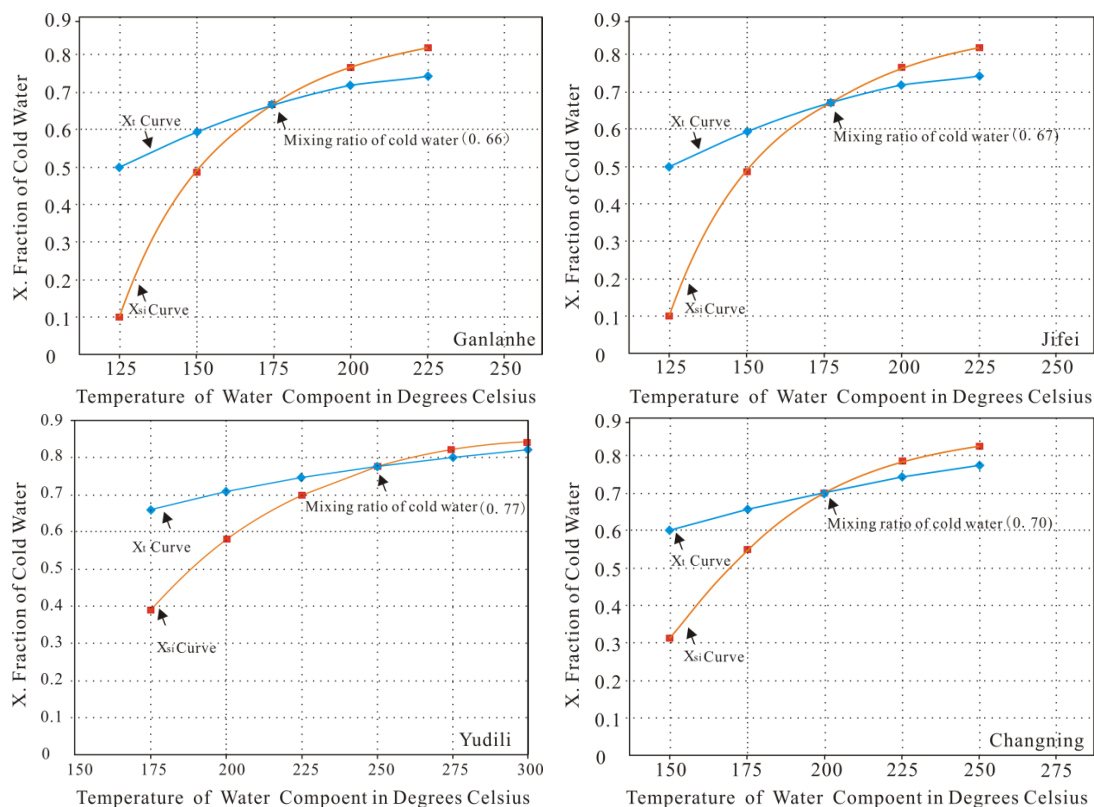


Figure 8. The fractions of cold water in the hot springs (Transverse axis-°C; Vertical axis-%)

Geochemical features of the hot springs

Oxygen isotope shift and water-rock interaction

The supply source of hot springs is generally determined through the comparison of global/local meteoric water line and H-O isotopes in the spring water (White et al., 2005; Dotsika et al., 2006; Han et al., 2015). The elevation effect of H-O isotopes can be used to calculate the recharge elevation of the hot springs, laying the basis for formation modelling of geothermal fields (Kose, 2007; Yamanaka et al., 2010).

Considering the conditions of the research area, δD and $\delta^{18}O$ can be adopted for the computation of the supply elevation. For high-temperature geothermal fields, the recharge sources are usually in remote or mountainous areas. Thus, the δD and $\delta^{18}O$ values of such fields are often lower than those of surface water and shallow groundwater (Zhou et al., 2009; Dotsika et al., 2010; Ba et al., 2018).

In view of the shift in $\delta^{18}O$ value (Figure 9) between the spring water and meteoric water line (Table 1), the author used $d\text{-excess} = \delta D - 8\delta^{18}O$ to calculate the exchange degree of $\delta^{18}O$. The $d\text{-excess}$ of the hot springs in the research area is shown in Figure 10, where the line of $d\text{-excess} = 10\text{‰}$ is the global meteoric water line proposed by Craig in 1961 (Kim et al., 1997; Zuo et al., 2014; Ingvar, 2016). It can be seen that the d values of the hot springs mostly fall between the $d = 0\text{‰}$ line and the $d = 10\text{‰}$ line, and stay close to the latter line as compared to the former line.

The difference between the hot springs in the $\delta^{18}O$ shift can be explained by their difference in vaporization and the mixing features of hot water and cold water.

The above results show that the $\delta^{18}\text{O}$ in the spring water equals that of meteoric water before shifting by 0.5~1.0%. Thus, the hot springs are recharged by meteoric water with $\delta^{18}\text{O}$ shifting, and the water-rock interaction conditions of the geothermal reservoir is relative closed. The significant isotope exchange in the hot springs can be attributed to the high temperature of geothermal reservoir and the long circulation distance (Fournier, 1977; Edmunds, 2004; Chandrajith et al., 2013).

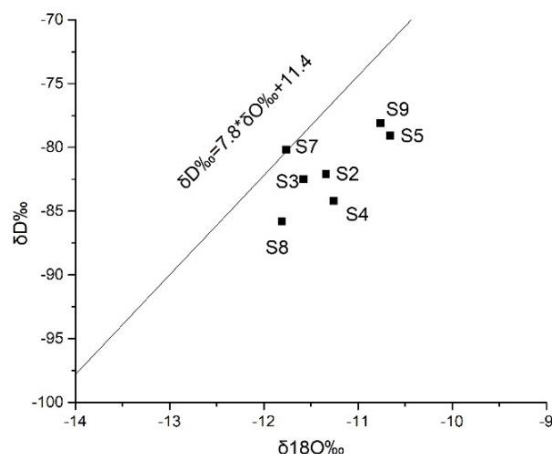


Figure 9. The δD and $\delta^{18}\text{O}$ compositions of the hot springs

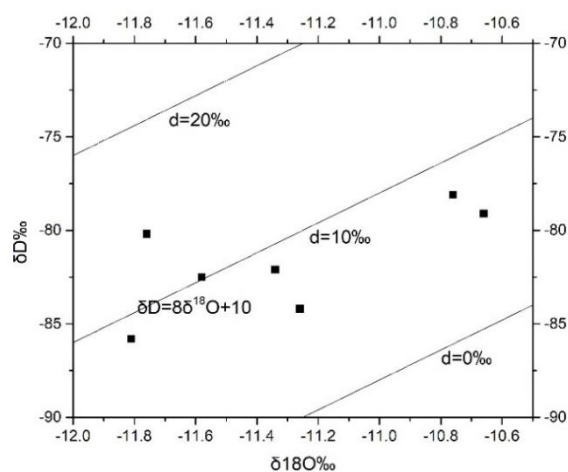


Figure 10. The δD - $\delta^{18}\text{O}$ values of the hot springs

According to the isotopic analysis, the δD and $\delta^{18}\text{O}$ values are close to meteoric water line. This means the hot springs agree with meteoric water in δD and $\delta^{18}\text{O}$ features. Besides, the lack of positive shift of $\delta^{18}\text{O}$ reflects a relatively low temperature of deep geothermal reservoir. Therefore, the hot springs are neither volcanic nor magmatic (Portugal et al., 2005; Chandrajith et al., 2013).

Considering the elevation effect of δD and $\delta^{18}\text{O}$, the groundwater elevation H (i.e. the height above sea level) can be defined as Eq.1:

$$H = (\delta_G - \delta_p) / k + h \quad (\text{Eq.1})$$

where h is the elevation of sampling point; δ_G is the $\delta^{18}\text{O}$ (δD) in the groundwater; δ_P is the $\delta^{18}\text{O}$ (δD) in the meteoric water around the sampling point; k is the elevation gradient of $\delta^{18}\text{O}$ (or δD) in the meteoric water (‰/100m). Using Equation (1), the H values of hot springs in the research area were computed with $K=-2.6\text{‰}/100\text{m}$ and $\delta\text{D}=-63.5\text{‰}$ (Xu et al., 2016).

The calculated results in Table 8 show that the meteoric water is the main recharge source of the hot springs; the recharge elevation lies between 1,549 and 2,403 m (mean value: 1,921 m); the supply elevation is positively correlated with the elevation of the spring mouth; the values of $\delta^{18}\text{O}$ and δD are linearly correlated. To sum up, the exposed hot springs are a mixture of low-temperature shallow groundwater and high-temperature deep groundwater. This conclusion echoes with the results of the hydro-chemical analysis.

Table 8. Elevation features of isotopic recharge area of groundwater in the research area

Hot Spring No.	$\delta\text{D}\text{‰}$	$\delta^{18}\text{O}\text{‰}$	Spring Mouth Elevation	H (m)
S2	-82.1	-11.34	943	1658.38
S3	-82.5	-11.58	1096	1826.76
S4	-84.2	-11.26	1020	1816.15
S5	-79.1	-10.66	949	1549.00
S7	-80.2	-11.76	1311	1953.30
S8	-85.8	-11.81	1546	2403.69
S9	-78.1	-10.76	1683	2244.53

Temperature of geothermal reservoir

The temperature of geothermal reservoir can be measured by “geochemical thermometers”, i.e. chemical contents and isotopes like SiO_2 , Na-K, Na-K-Ca and $\delta^{18}\text{O}$ in sulphate (Zhang et al., 2008; Zhou et al., 2009).

Here, the Na-K-Mg triangular diagram is employed to judge if cationic geochemical thermometers are suitable for the hot springs (Giggenbach, 1988). As shown in Figure 11, all the water samples through the corner of $\text{Mg}^{0.5}$, reflecting the high Mg^{2+} content in the samples and its impacts on the calculation of geochemical thermometers. Thus, SiO_2 geochemical thermometers are the best choice to calculate the temperature of our geothermal reservoirs.

In this way, it is learned that the geothermal reservoir temperatures of S2 and S5 are 100.1 and 79.8°C, respectively; the mean annual temperature in the research area is 19.5°C, with a geothermal gradient of 20 m/°C. Setting the annual constant temperature to 30 m, the SiO_2 geochemical thermometer without vapor loss T_1 and the chalcedony geochemical thermometer T_2 can be respectively calculated as Eq.2 and Eq.3:

$$T_1 = 1309 / (5.19 - \text{Lg}C_{\text{SiO}_2}) - 273.15 \quad (\text{Eq.2})$$

$$T_2 = 1032 / (4.69 - \text{Lg}C_{\text{SiO}_2}) - 273.15 \quad (\text{Eq.3})$$

where T is the temperature of geothermal reservoir; C_{SiO_2} is the mass concentration of SiO_2 (mg/L). According to the calculated results in Table 9, the temperatures of our

geothermal reservoirs belong to the interval of 80~146°C, with the mean value of 111.8°C. Thus, there is a great potential for exploitation of geothermal resources in the research area.

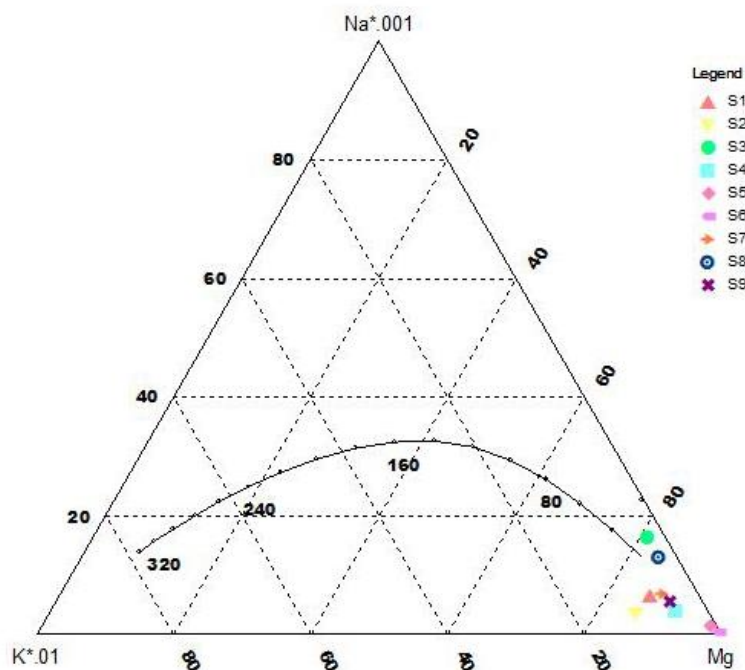


Figure 11. Na-K-Mg triangular diagram of the hot springs

Table 9. Calculation results of geothermal reservoir temperature (°C)

Sample	SiO ₂ (mg/L)	Equation (2)	Equation (3)	Temperature
S2	48.26	100.16	70.11	71.0
S3	73.58	120.74	92.38	82.0
S4	70.37	118.45	89.89	80.0
S5	30.33	79.86	48.53	44.0
S7	117.22	146.26	120.59	73.0
S8	42.65	94.54	64.10	42.5
S9	89.97	131.37	104.06	58.0

Conclusions

The geothermal fields in the research area are controlled by the primary and secondary faults. At the intersections between the faults, the clastic sediments in the Cenozoic depression provide a good thermal cover for the geothermal reservoirs. The Kejie Fault controls the sedimentation, metamorphism and magmatic activities since the Early Paleozoic era. The control effect is particularly prominent in Late Paleozoic era. The C-M Structural Belt controls the distribution of geothermal resources in the eastern part of the research area.

The temperature of the hot springs in the research area can reach 90°C. The water of all the hot springs has good quality, belongs to the hydro-chemical type of HCO₃-Na,

and shares the same recharge source and stable formation conditions. These hot springs provide typical fault-controlled geothermal resources.

The meteoric water is the main supply source of the hot springs; the recharge elevation lies between 1,549 and 2,403 m (mean value: 1,921 m); the recharge elevation is positively correlated with the elevation of the spring mouth; The cold-water fractions in S3, S4, S7 and S1 fall in the range of 66%~77%; the temperatures of our geothermal reservoirs belong to the interval of 80~146°C, with the mean value of 111.8°C, which are controlled by Kejie Fault and C-M Structural Belt.

In the hot springs, the dissolved inorganic carbon exists as HCO_3^- , and the $\delta^{13}\text{C}_{\text{DIC}}$ value is similar to the value of $\delta^{13}\text{C}_{\text{HCO}_3^-}$; the δD and $\delta^{18}\text{O}$ features are the same as those of meteoric water; the lack of positive shift of $\delta^{18}\text{O}$ reflects a relatively low temperature of deep geothermal reservoir, meaning that the hot springs are neither volcanic nor magmatic; the significant isotope exchange in the hot springs can be attributed to the high temperature of geothermal reservoir and the long circulation distance.

The ^{14}C isotopic dating shows that the hot springs in the eastern part and S4 are respectively aged $17,220\pm 550\text{a}$ and $16,510\pm 1,600\text{a}$. The C-M Structural Belt has a longer groundwater circulation path than Kejie Fault. Despite the slight difference in activities and formation causes, the hot springs in both western and eastern parts of the research area were recharged by paleo-precipitation recharge before Late Pleistocene.

The geothermal resources have great potential for development in the study area. It is necessary to conduct deep drilling, evaluation and scientific research to identify the potential of resources and provide scientific basis for development and utilization planning.

The potential assessment of geothermal resources in the study area is still in a stable state. It is necessary to strengthen exploration, research and monitoring, accelerate the development and utilization of geothermal energy in deep fault zone, promote the release of energy in fault zone and reduce the risk of earthquake occurrence.

Acknowledgements. This research was supported by the National Key Research and Development Program of China (No. 2018YFC0604301), the Guangxi Natural Science Foundation (No.2018GXNSFAA294046, NO.2017GXNSFAA198208), the National key Research and Development Program of China (No.2017YFC0406104) and the Geological survey project of China (No. DD20190562).

REFERENCES

- [1] Ahmadi, M. H., Ramezanizadeh, M., Nazari, M. A., Lorenzini, G., Kumar, R., Jilte, R. (2018): Applications of nanofluids in geothermal: A review. – *Mathematical Modelling of Engineering Problems* 5(4): 281-285.
- [2] Awaleh, M. O., Hoch, F. B., Boschetti, T., Soubaneh, Y. D., Egueh, N. M., Elmi, S. A. (2015): The geothermal resources of the republic of djibouti – ii: geochemical study of the lake abhe geothermal field. – *Journal of Geochemical Exploration* 159(6): 129-147.
- [3] Ba, J. J., Su, C. T., Li, Y. Q. (2018): Characteristics of heat flow and geothermal fields in Ruidian, Western Yunnan Province, China. – *International Journal of Heat and Technology* 36(4): 1203-1211.
- [4] Ba, J. J., Su, C. T., Li, Y. Q. (2018): A case study on heat source mechanism of high-temperature geothermal field. – *Annales de Chimie Science des Matériaux* 42(1): 129-147.

- [5] Brown, K. L., Simmons, S. F. (2003): Precious metals in high-temperature geothermal systems in New Zealand. – *Geothermics* 32(4): 619-625.
- [6] Chandrajith, R., Barth, J. A. C., Subasinghe, N. D., Merten, D., Dissanayake, C. B. (2013): Geochemical and isotope characterization of geothermal spring waters in Sri Lanka: evidence for steeper than expected geothermal gradients. – *Journal of Hydrology (Amsterdam)* 476(7): 360-369.
- [7] Dotsika, E., Leontiadis, I., Poutoukis, D. (2006): Fluid geochemistry of the Chios geothermal area, Chios Island, Greece. – *Journal of Volcanology and Geothermal Research* 154(3-4): 237-250.
- [8] Dotsika, E., Poutoukis, D., Raco, B. (2010): Fluid geochemistry of the Methana peninsula and Loutraki geothermal area, Greece. – *Journal of Geochemical Exploration* 104(3): 97-104.
- [9] Du, J., Liu, C., Fu, B. (2005): Variations of geothermometry and chemical–isotopic compositions of hot spring fluids in the Rehai geothermal field, southwestern China. – *Journal of Volcanology & Geothermal Research* 142: 243-261.
- [10] Edmunds, W. M. (2004): Bath thermal waters: 400 years in the history of geochemistry and hydrology. – *200 Years of British Hydrogeology* 225(1): 193-199.
- [11] Fournier, R. O. (1977): Chemical geothermometers and mixing models for geothermal systems. – *Geothermics* 5: 41-50.
- [12] Giggenbach, W. F. (1988): Geothermal solute equilibria. Derivation of Na-K-Mg-Ca bioindicators. – *Geochimica et Cosmochimica Acta* 52(12): 2749-2765.
- [13] Guo, Q. H. (2012): Hydrogeochemistry of high-temperature geothermal systems in China: A review. – *Applied Geochemistry* 27(10): 1887-1898.
- [14] Guo, S. Y., Li, X. J. (2013): Reservoir stratum characteristics and geothermal resources potential of Rongcheng uplift geothermal field in Baoding, Hebei. – *Chinese Journal of Geology* 48(3): 922-931.
- [15] Han, K., Gan, F. P., Chen, Y. L. (2015): The structure characteristics and geological significance in the northern segment of Kejie Fault. – *Progress in Geophysics (in Chinese)* 30(1): 70-76.
- [16] Ingvar, B. F. (2016): Geothermal energy for the benefit of the people. – *Renewable and Sustainable Energy Reviews* 3: 299-312.
- [17] Kim, S. T., O'Neil, J. R. (1997): Equilibrium and nonequilibrium oxygen isotope effects in synthetic carbonates. – *Geochimica et Cosmochimica Acta* 61(16): 3461-3475.
- [18] Kose, R. (2007): Geothermal energy potential for power generation in Turkey: A case study in Simav, Kutahya. – *Renewable and Sustainable Energy Reviews* 11(3): 497-511.
- [19] Lachenbruch, A. H., Sass, J. H. (2013): The stress heat-flow paradox and thermal results from Cajon Pass. – *Geophysical Research Letters* 15(9): 981-984.
- [20] Mawarni, L. W., Maryanto, S., Nadhir, A. (2018): Magnetic method used in geothermal reservoirs identification in Kasinan-Songgoriti, East Java, Indonesia. – *Environmental and Earth Sciences Research Journal* 5(4): 87-93.
- [21] Mongillo, M. A. (2010): Preface to geothermics special issue on sustainable geothermal utilization. – *Geothermics* 39(4): 279-282.
- [22] Olivier, J., Venter, J., Jonker, C. S. (2011): Thermal and chemical characteristics of hot water springs in the northern part of the Limpopo province, South Africa. – *Water SA* 37(4): 427-436.
- [23] Portugal, E., Sandoval, F., Barragan, R. M. (2005): Isotopic ($\delta^{18}\text{O}$, δD) patterns in Los Azufres (Mexico) geothermal fluids related to reservoir exploitation. – *Geothermics* 34(4): 527-547.
- [24] Wang, G. L., Zhang, F. W., Liu, Z. M. (2000): An analysis of present situation and prospects of geothermal energy development and utilization in the world. – *Acta Geoscientia Sinica* 2: 134-139.
- [25] White, P. A., Hunt, T. M. (2005): Simple modelling of the effects of exploitation on hot springs, Geysir Valley, Wairakei, New Zealand. – *Geothermics* 34(2): 184-204.

- [26] Xu, S. G., Ba, J. J., Chen, X. F. (2016): Predicting Strata Temperature Distribution from Drilling Fluid Temperature. – *International Journal of Heat and Technology* 34(2): 345-350.
- [27] Yamanaka, T., Shimada, J., Hamada, Y. (2010): Hydrogen and oxygen isotopes in precipitation in the northern part of the North China Plain: climatology and inter-storm variability. – *Hydrological Processes* 18(12): 2211-2222.
- [28] Zhang, G. P., Liu, C. Q., Liu, H. (2008): Geochemistry of the Rehai and Ruidian geothermal waters, Yunnan Province, China. – *Geothermics* 37(1): 73-83.
- [29] Zhou, X., Fang, B., Zhou, H. Y. (2009): Isotopes of deuterium and oxygen-18 in thermal groundwater in China. – *Environmental Geology* 57(8): 1807-1814.
- [30] Zuo, Y. H., Qiu, N. S., Hao, Q. Q. (2014): Present Geothermal Fields of the Dongpu Sag in the Bohai Bay Basin. – *Acta Geologica Sinica (English Edition)* 3: 915-930.